https://doi.org/10.5194/egusphere-2026-5594
Preprint. Discussion started: 6 November 2026
© Author(s) 2026. CC BY 4.0 License.

Technical Note: Ionospheric Boundaries Derived from Partial Auroral Images

Angeline Burrell[1], Gareth Chisham[2], Bruce Fritz[1], Yun-Ju Chen[3], and Kate Zawdie[1]

[1]U.S. Naval Research Laboratory, 4555 Overlook Ave. SW, Washington, D.C., U.S.A., 20375
[2]British Antarctic Survey, Cambridge, UK
[3]University of Texas at Dallas, Richardson, Texas, USA

Correspondence: Angeline G. Burrell (angeline.g.burrell.civ@us.navy.mil)

Abstract. The high latitudes are a distinct region of the geospace environment, where strong coupling between the atmosphere, ionosphere, magnetosphere, and solar wind create distinct regions where different physical processes dominate. Because of this, modelling and statistical studies of the geospace environment at high latitudes should avoid mixing data measured in different regions (e.g., the polar cap, the auroral oval, and the sub-auroral regions). This study presents two new sets of poleward and equatorward Auroral Luminosity Boundaries (ALBs) along with functional definitions that relate these ALBs to the poleward and equatorward particle precipitation boundaries that mark the open–closed magnetic field line boundary (OCB) that demarcates the transition between the polar cap and auroral oval and the diffuse auroral boundary at the equatorward edge of the auroral oval. These data sets are obtained from space-based auroral imagers flown on the Thermosphere Ionosphere Mesosphere Energetics and Dynamics (TIMED) satellite and the Defense Meteorological Satellite Program (DMSP) constellation, that observe slices of the auroral oval in both hemispheres. The validation of the derived OCB locations against an independent polar cap proxy shows that the ALBs identified at the Lyman-Birge-Hopfield (LBH) Long wavelengths may be used together with other auroral boundary data sets in scientific studies.

1 Introduction

The high-latitude ionosphere is a region shaped by the strong coupling between the solar wind, magnetosphere, ionosphere, and neutral atmosphere. One of its major features, the auroral oval, is highly responsive to changes in the Interplanetary Magnetic Field (IMF) that is embedded in the solar wind (e.g., Akasofu, 1966; Dungey, 1961). The motion of the poleward boundary of the auroral oval is coupled to that of the Open-Closed field line Boundary (OCB), which marks the change from terrestrial magnetic field lines that are connected to the IMF (open field lines) and those that connect back into the planet (closed field lines) (Cowley and Lockwood, 1992). The Equatorward Auroral Boundary (EAB) maps to the equatorward edge of the magnetospheric plasma sheet (e.g., Borovsky and Valdivia, 2018; Troyer et al., 2025). Both of these locations move in response to changing conditions in the solar wind and magnetosphere, and demarcate distinct physical regimes in the high-latitude ionosphere and thermosphere (e.g., Decotte et al., 2023; Chisham et al., 2025; Mukhopadhyay et al., 2025, and references therein).

https://doi.org/10.5194/egusphere-2026-5594
Preprint. Discussion started: 6 November 2026
© Author(s) 2026. CC BY 4.0 License.

Prior studies have established magnetic local time (MLT) dependent relationships between the poleward and equatorward auroral luminosity boundaries (ALBs) observed in Far Ultraviolet (FUV) wavelengths, and direct observations of the OCB and EAB measured by changes in the magnetospheric particle precipitation (Carbary et al., 2003; Longden et al., 2010; Burrell et al., 2020; Chisham et al., 2022). This study builds on this body of work by providing similar MLT-dependent functions for the Lyman-Birge-Hopfield (LBH) Long and Short wavelength ALBs identified in images from the Thermosphere Ionosphere Mesosphere Energetics and Dynamics (TIMED) Global Ultraviolet Imager (GUVI) and the Defense Meteorological Satellite Program (DMSP) Special Sensor Ultraviolet Spectrographic Imager (SSUSI). The OCB corrections for each instrument and wavelength band are validated, allowing comparisons with prior studies.

This article is organised as follows. The imager data sets from TIMED and DMSP that are used in this study are described in Section 2. The methodology for the derivation of the OCB and EAB boundary corrections, and its implementation, are presented in Section 3. The validation of the OCB determination is shown in Section 4. The conclusions are presented in Section 5.

2 Data

Both the TIMED/GUVI and DMSP/SSUSI instruments scan the satellite's cross-track from horizon to horizon and measures auroral emissions in five different spectral bands: HI (121.6 nm), OI (130.4nm), OI (135.6nm), LBH Short (LBHS, 141-152.8nm), and LBH Long (LBHL, 167.2-181.2nm). (Paxton et al., 2004). For this study, high resolution Level 1C imaging data files were obtained from the NASA Space Physics Data Facility (SPDF) using pysatNASA (Klenzing et al., 2024) . LBHS and LBHL emissions, in particular, are both optically thin and generated by particle impact excitation and may therefore be used as a visual indicator of auroral particle precipitation. Sections 2.1 and 2.2.1 describe the unique attributes of each imager as well as the specific datasets used to determine the auroral luminosity boundaries calibrated to the OCB and EAB. The luminosity geolocation can be calibrated with the energetic particle measurements described in Section 2.2.2 . The luminosity boundary locations are further validated through comparison against a separate physical mechanism, the convection reversal boundary, as described in Section 2.2.3.

2.1 TIMED GUVI

TIMED is a NASA funded satellite mission whose goal is to study the lower portion of the Earth's upper atmosphere. The TIMED satellite was launched on 7 Dec 2001, into an orbit with an altitude of 625 km, an inclination of 74.1°, and a period of 97.3 minutes (Yee et al., 1999). The TIMED GUVI observations used in this study from the start of data collection in 17 Feb 2002 through 10 Dec 2007.

Poleward and equatorward auroral luminosity boundary locations were obtained for this time period from the LBHS and LBHL spectral bands using pyIntensityFeatures (Burrell et al., 2025, 2026b). These boundaries may be accessed online (Burrell and Zawdie, 2026). Figure 1 shows the distribution of locations where ALBs were detected for the GUVI LBHL and LBHS auroral scans in AACGMV2 magnetic coordinates (Shepherd, 2014; Burrell et al., 2018) for the northern and southern

https://doi.org/10.5194/egusphere-2026-5594
Preprint. Discussion started: 6 November 2026
© Author(s) 2026. CC BY 4.0 License.

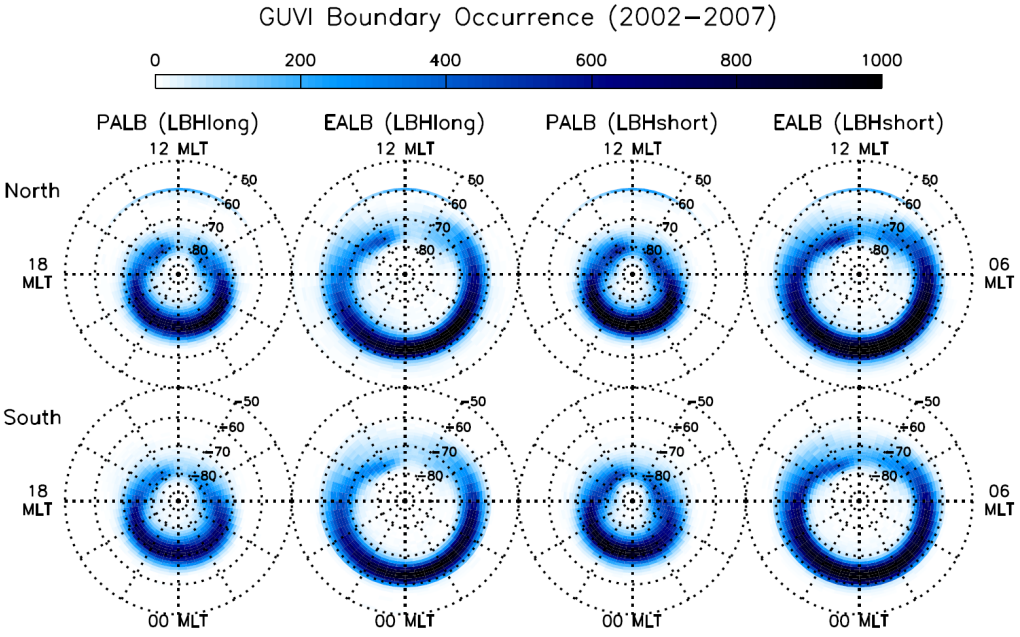


Figure 1. The GUVI LBHL (left two columns) and LBHS (right two columns) ALB occurrence for 2002-2007 separated by boundary type (PALB and EALB) and hemisphere.

hemispheres. The figure shows that the distributions of boundaries for the LBHL and LBHS bands are very similar, with the Equatorward ALB (EALB) distributions being centred approximately 10° equatorward of the Poleward ALB (PALB) distributions. The northern hemisphere distribution is characterised by a thin band of anomalous measurements around 60°. This band has been removed from all further analysis.

2.2 DMSP

DMSP is a U.S. Department of Defense mission designed to monitor the Earth's meteorological, oceanographic, and solar-terrestrial physics environments. The first DMSP satellite was launched in 1962, and there are currently several satellites operational and in their desired orbits with alpha-numeric designators of F1-F19. These orbits are sun-synchronous, polar orbits (inclinations > 97°) with altitudes near 830 km. Each satellite crosses the equatorial plane at a different Solar Local Time (SLT). The payload onboard each satellite varies, as do their orbits.

2.2.1 SSUSI

The SSUSI instrument was launched onboard the DMSP F16-F19 satellites. The first SSUSI measurements were obtained from F16 starting on 30 Oct 2003 and F18 continued to provide observations into 2025. In contrast to GUVI, SSUSI scans cross-track to the satellite orbit from the horizon opposite to the sun up to the tangent point (Paxton et al., 2002).

https://doi.org/10.5194/egusphere-2026-5594
Preprint. Discussion started: 6 November 2026
© Author(s) 2026. CC BY 4.0 License.

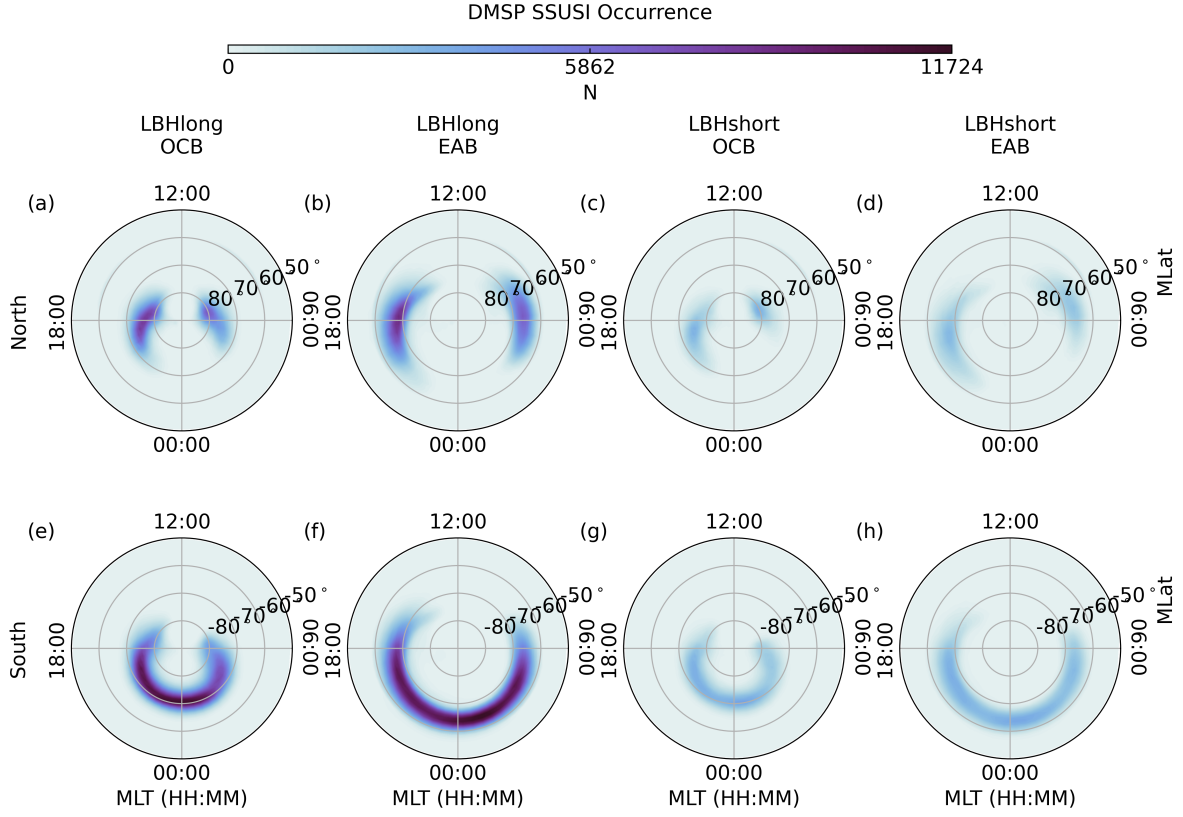


Figure 2. SSUSI ALB occurrence by boundary, wavelength channel, and hemisphere. The northern hemisphere is on the top row and the southern hemisphere is on the bottom row. LBHL is in the left two columns and LBHS is in the right two columns. The poleward ALBs are in panels a, c, e, and g, while the equatorward ALBs are in panels b, d, f, and h. In each panel all available DMSP spacecraft are combined.

For this study, the high-resolution Level 1C imaging data files were obtained from NASA SPDF using pysatNASA from 1 Jan 2005 through 31 Dec 2023. As with the GUVI data, the poleward and equatorward ALB locations were obtained for this time period from the LBHS and LBHL spectral bands using pyIntensityFeatures. These boundaries may be accessed online (Burrell et al., 2026a). The distribution of these boundaries by spectral band, hemisphere, and boundary type (OCB/EAB) are shown in Figure 2. To reduce the impact of orbit on the boundaries, the MLT distribution of boundaries in each hemisphere were examined across 2005-2024 and limits established at MLTs where less than 100 boundaries were observed in the LBHL. This reduces the impact of edge effects (quality issues that are less likely to be removed by outlier detection due to their location at the edge of the image) in the boundary selection. These limits are presented in Table **??**.

https://doi.org/10.5194/egusphere-2026-5594
Preprint. Discussion started: 6 November 2026
© Author(s) 2026. CC BY 4.0 License.

Satellite ID	Hemisphere	Good MLT Range
F16	North	03:15-10:30 and 13:45-22:30
	South	13:45-07:45
F17	North	02:45-10:00 and 14:15-21:00
	South	14:45-08:15
F18	North	03:35-10:30 and 13:15-22:30
	South	13:45-07:45
F19	North	03:45-09:00 and 16:15-21:00
	South	16:45-06:15

Table 1. SSUSI MLT selection to reduce the impact of edge effects on boundary selection.

2.2.2 SSJ

The DMSP Special Sensor J (SSJ) 4 and 5 were designed to measure the characteristics of ions and electrons precipitating into the auroral region and polar cap. This study uses two different sources of DMSP SSJ auroral boundaries: those compiled by Newell et al. (2004), which distinguishes between different particle precipitation regions, and the poleward and equatorward boundaries identified using an automated process by Kilcommons et al. (2017). Both of these data sets directly measure the EAB and OCB, and so are used as the calibration source for the GUVI and SSUSI ALBs, respectively.

As recommended by Newell et al. (2004), the b1e/b2s (nightside) and deq (dayside) boundaries are used to identify the EAB and the b6 (nightside) and doc (dayside) boundaries are used to identify the OCB (Newell et al., 1991, 1996). This data set is nominally available online CITE, and the dates used in this project cover the GUVI ALBs. Because these measurements directly provide the OCB and EAB locations and do not have any uncertainties associated with them, their fidelity needs to be assessed by considering DMSP orbital characteristics (Chisham et al., 2022). Figure 3 shows a comparison of the distribution of DMSP and GUVI boundaries. The red coned regions mark out the areas where boundary comparisons are utilized in this study. Here, the derived particle precipitation boundaries may be unreliable due to the orientation of the satellite orbit (e.g., when the orbit is closely aligned with the boundary) (see Chisham et al. (2022) for details). Additionally, boundaries from F16 and F17 are not used as their overall spatial distribution differs significantly from those of the other DMSP spacecraft. This is to reduce the number of anomalous comparisons in the data set. F18 data were not readily available in this database.

The more recent DMSP boundary estimation process developed by Kilcommons et al. (2017) used updated ephemera to correct high-latitude geolocation errors and found the edges of the auroral precipitation using a threshold identification process. Each boundary location is accompanied by a Figure of Merit (FoM), that specifies the level of confidence in the identification. These boundaries are available from 2010-2014 (Kilcommons et al., 2019), and are used to calibrate the SSUSI ALBs during this time period. Following the recommendations of prior research using this data set (Burrell et al., 2020), this study removed DMSP SSJ OCB and EAB detections with a FoM < 3, as well as those boundaries that fell near the edge of the DMSP orbits (determined by examining the magnetic local time distributions of boundary detections for each spacecraft and choosing only

https://doi.org/10.5194/egusphere-2026-5594
Preprint. Discussion started: 6 November 2026
© Author(s) 2026. CC BY 4.0 License.

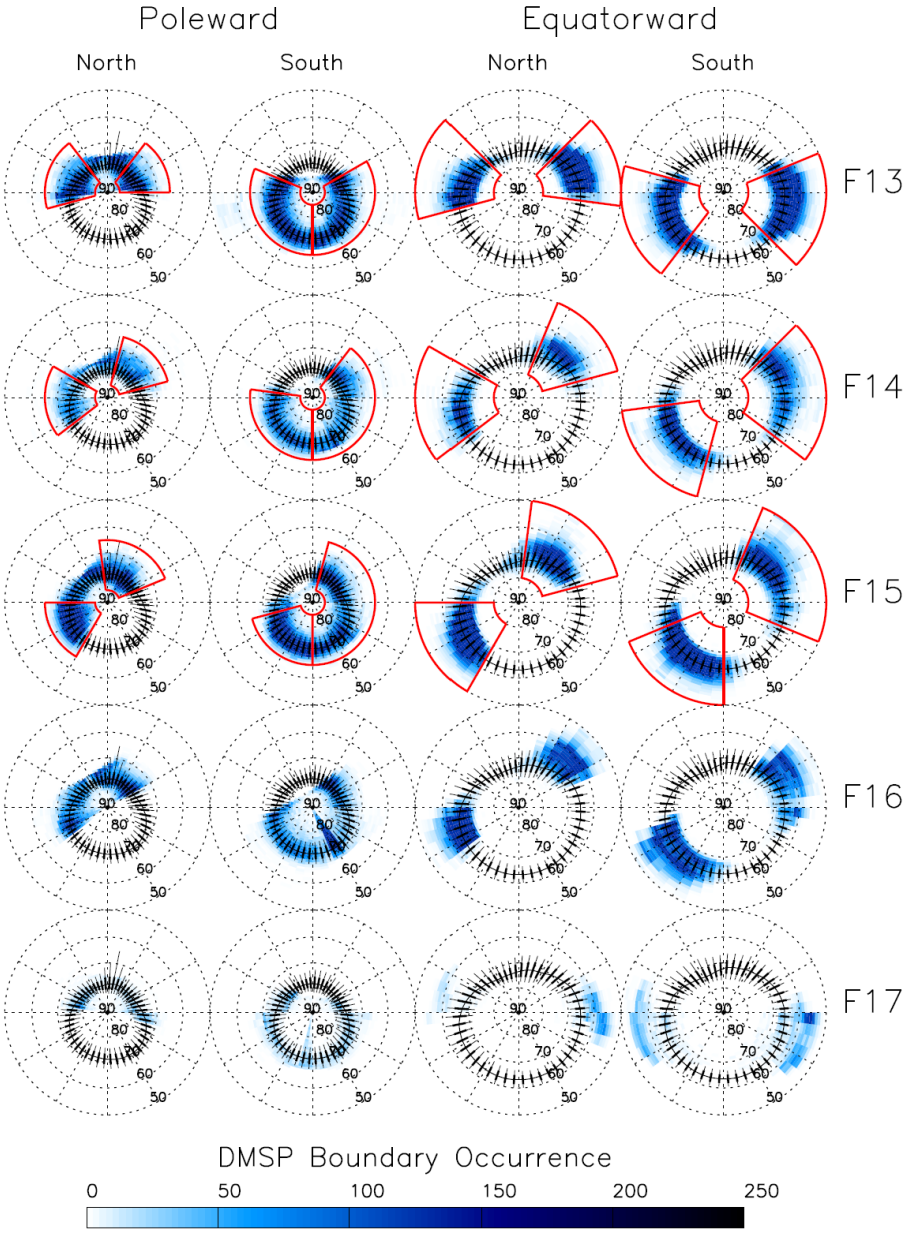


Figure 3. DMSP OCB and EAB location occurrence by spacecraft and hemisphere (blue) in AACGM co-ordinates. The median GUVI poleward and equatorward ALB locations are shown in black, with thick bars marking the interquartile range, and thin bars marking the 10 and 90% percentilles. The red wedges enclose the regions where the DMSP Newell boundary estimations are wholly reliable. Boundaries outside of these regions are removed to reduce the impact of orbit artifacts.

https://doi.org/10.5194/egusphere-2026-5594
Preprint. Discussion started: 6 November 2026
© Author(s) 2026. CC BY 4.0 License.

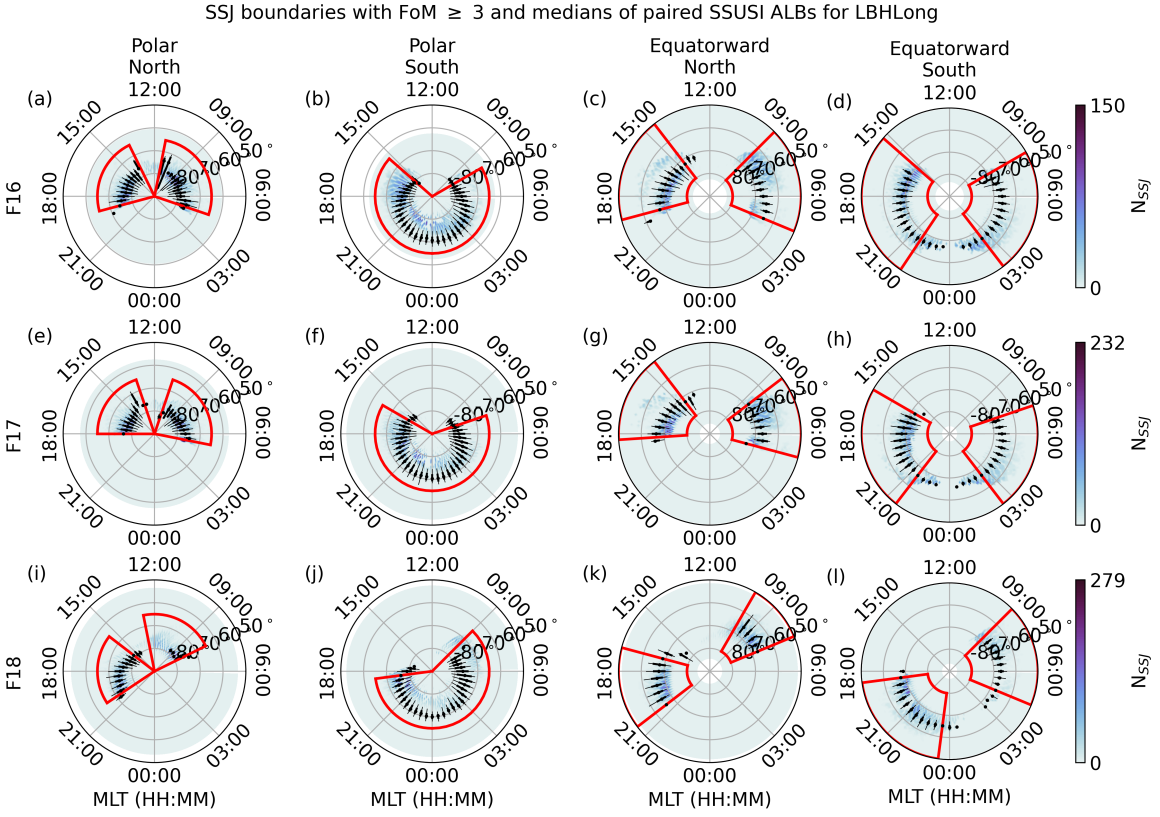


Figure 4. Northern hemisphere DMSP SSJ boundary occurrence (blue points) and SSUSI LBHS median ALB locations (black dots) for the poleward (left) and equatorward (right) boundaries for each DMSP spacecraft (labeled for each row).

times with 100 or more boundary detections). These limits are marked by the red cones in Figure 4. This figure also shows distribution of the high FoM SSJ data along with the median locations of the SSUSI ALBs that were paired to the SSJ data prior to the orbital selections were made.

In all of these figures (Figure 3 and 4) the intensity of the blue shading denotes areas with more DMSP SSJ boundary detections, the black dots or solid lines shows the median location of the ALBs, the thick bars mark the upper and lower quartiles, and the thin bars mark the extent from the 90^{th} to the 10^{th} percentiles. This shows that in regions where both boundaries have data the ALB locations are typically better constrained and that the MLT coverage is better in the southern hemisphere.

2.2.3 SSIES

The DMSP Special Sensor for Ions, Electrons, and Scintillation (SSIES), an ion velocity meter, was flown onboard the DMSP satellites F08-F18 (Hall, 2001). Amongst other in situ plasma quantities, the SSIES instruments measure the perpendicular and

https://doi.org/10.5194/egusphere-2026-5594
Preprint. Discussion started: 6 November 2026
© Author(s) 2026. CC BY 4.0 License.

ram ion velocities. This makes it possible to identify the location of the Convection Reversal Boundary (CRB) (Chen et al., 2015).

For this study, CRBs were derived using the method outlined by Chen et al. (2015). As in prior studies, they are used to validate the OCB corrections applied to the poleward ALBs within an hour of dawn (06:00 MLT) and dusk (18:00 MLT) (Burrell et al., 2020; Chisham et al., 2022). The CRB data set was cleaned by removing observations made at times characterised by low ion density (Chen et al., 2015; Chen and Heelis, 2018) or complex plasma convection. More details about the CRB dataset can be found in Burrell et al. (2020).

3 Boundary Correction

The process to calculate the boundary calibrations between the poleward ALB and the OCB, as well as between the equatorward ALB and the EAB follows the method laid out by Boakes et al. (2008) when determining the relationship between the IMAGE FUV poleward ALBs and the OCB. It follows four steps:

1. identify the SSUSI and GUVI ALBs,
2. pair the SSUSI and GUVI ALBs with the DMSP SSJ OCB and EAB measurements,
3. determine the typical offset between the ALB and the OCB/EAB locations at a given MLT, and
4. find a functional fit for the offset variation with MLT for each FUV wavelength band and instrument.

The functional fit may then be applied to the GUVI or SSUSI ALBs. This permits the GUVI and SSUSI boundaries to be used more easily in combination with other high-latitude boundary data sets and for studies that examine atmosphere-ionosphere-magnetosphere interactions. In this study, a second order spherical harmonic fit was used, consistent with prior imager studies (Carbary et al., 2003; Chisham et al., 2022).

$$L(\lambda) = A_0 + A_1 \cos(\lambda + \alpha_1) + B_1 \sin(\lambda + \beta_1) + A_2 \cos 2(\lambda + \alpha_2) + B_2 \sin 2(\lambda + \beta_2) \quad (1)$$

The first step was accomplished using pyIntensityFeatures, as discussed in Sections 2.1 and 2.2.1. Each of these ALBs, whose distributions were shown in Figures 1 and 2, have uncertainties related to the quality of the fits used to identify the boundary locations.

When pairing the DMSP OCB and EAB boundaries from either Newell et al. (2004) or Kilcommons et al. (2017) with the GUVI and SSUSI ALBs, respectively, time and longitude/MLT were used to correlate measurements between spacecraft. For all instruments the boundary detections must have occurred within 10 min of Universal Time (UT) and 15 min of MLT. All DMSP spacecraft were considered in any combination (for example, SSUSI data from F16 may be paired with SSJ data from any DMSP spacecraft). The paired boundaries were then differenced, as shown in equation 2.

$$\Delta\phi = |\phi_{ALB}| - |\phi_{SSJ}| \quad (2)$$

https://doi.org/10.5194/egusphere-2026-5594
Preprint. Discussion started: 6 November 2026
© Author(s) 2026. CC BY 4.0 License.

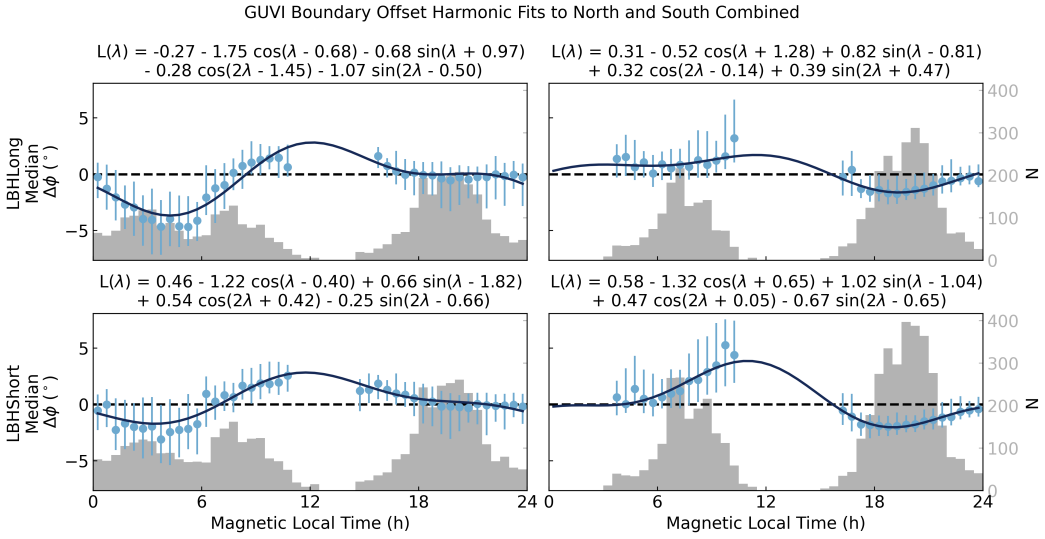


Figure 5. Poleward (left) and equatorward (right) boundary offset (GUVI - Newell) fits for the SSUSI LBHL (top) and LBHS (bottom). Medians and interquartile ranges of the offsets are plotted by blue circles and bars, the fit is plotted as dark blue line, and the data availability is shown as a grey histogram.

In the above equation, ϕ denotes the magnetic latitude, the ALB subscript indicates the latitude is from the GUVI or SSUSI poleward or equatorward ALB, and the SSJ subscript indicates that the latitude is from the SSJ OCB or EAB. The absolute values are necessary to combine the differences from the two hemispheres. The GUVI and SSUSI $\Delta\phi$ were grouped into 30 min bins to find the median values. These latitude differences were then fit using Levenberg-Marquardt least-squares minimisation to identify the coefficients in Equation 1. The medians, upper quartiles, and lower quartiles of these latitude differences are plotted in Figures 5 and 6 as markers with bars. The results of the spherical harmonic fits are overplotted using solid lines and the data availability in each MLT bin is shown as a histogram.

Only medians from half-hourly bins with more than 20 points were used to constrain the fit for GUVI and SSUSI. For the SSUSI data, all DMSP satellites were combined to achieve the best MLT coverage. This was necessary because the SSUSI field-of-view is smaller than that of GUVI. However, it is still desirable to have individual instrument corrections for each SSUSI imager. To achieve this result given the MLT restrictions, the median difference between the $\Delta\phi$ measurements for each SSUSI imager and the spherical harmonic fit shown in Figure 6 was calculated. This difference is applied as an offset, as illustrated in Figure 7. The final spherical harmonic coefficients for both GUVI and SSUSI are tabulated in Table 2, with the SSUSI A_0 values incorporating the satellite offsets presented in Figure 7.

https://doi.org/10.5194/egusphere-2026-5594
Preprint. Discussion started: 6 November 2026
© Author(s) 2026. CC BY 4.0 License.

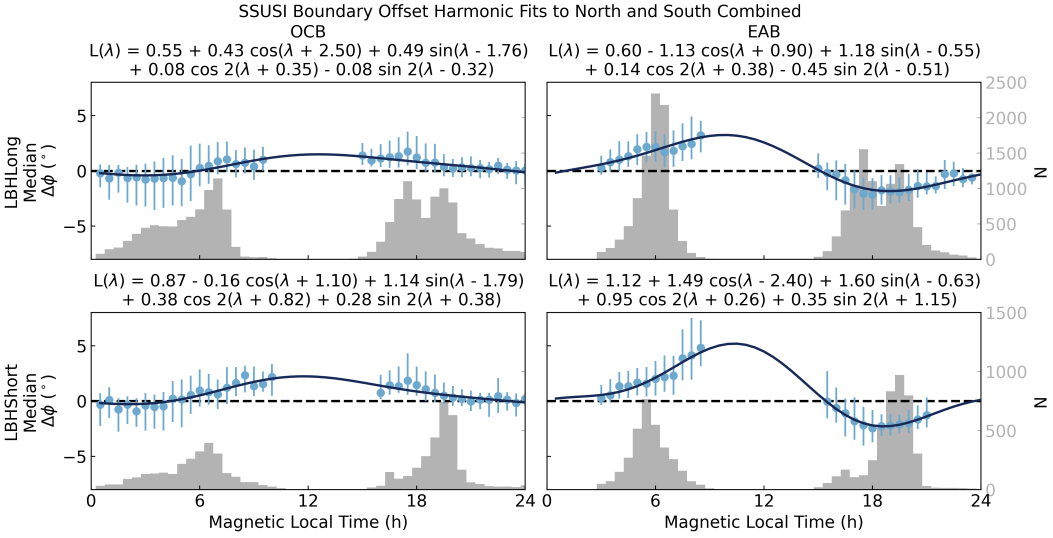


Figure 6. Poleward (left) and equatorward (right) boundary offset (SSUSI - SSJ) fits for the SSUSI LBHL (top) and LBHS (bottom). Medians and interquartile ranges of the offsets are plotted by blue circles and bars, the fit is plotted as dark blue line, and the data availability is shown as a grey histogram.

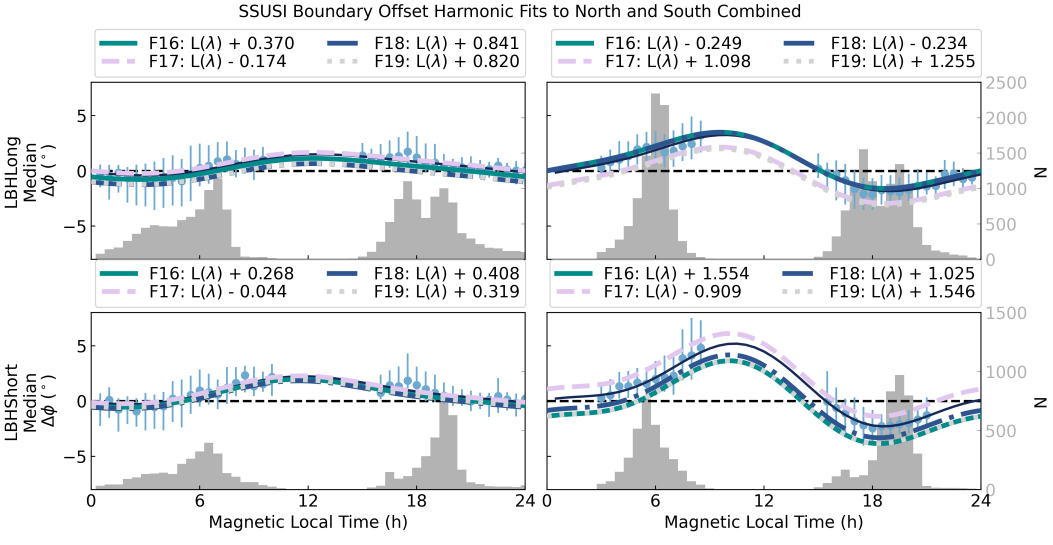


Figure 7. Poleward (left) and equatorward (right) boundary offset (SSUSI - SSJ) fits for the SSUSI LBHL (top) and LBHS (bottom). Medians and interquartile ranges of the offsets are plotted by blue circles and bars, the fits for each DMSP spacecraft are plotted as lines (f16 is in solid teal, f17 is the dashed light purple, f18 is dot-dashed blue, and f19 is dotted light grey), and the total data availability is shown as a grey histogram.

https://doi.org/10.5194/egusphere-2026-5594
Preprint. Discussion started: 6 November 2026
© Author(s) 2026. CC BY 4.0 License.

Table 2. Spherical harmonic coefficients for $\Delta\phi$

Instrument	Channel	Boundary	A_0	A_1	α_1	B_1	β_1	A_2	α_2	B_2	β_2
GUVI	LBHS	EAB	0.5833	-1.3184	0.6462	1.0221	-1.0449	0.4660	0.0534	-0.6739	-0.6547
		OCB	0.4636	-1.2181	-0.3994	0.6575	-1.8204	0.5426	0.4189	-0.2475	-0.6644
	LBHL	EAB	0.3136	-0.5196	1.2754	0.8204	-0.8073	0.3215	-0.1361	0.3900	0.4684
		OCB	-0.2727	-1.7452	-0.6807	-0.6801	0.9749	-0.2810	-1.4526	-1.0674	-0.4985
SSUSI F16	LBHS	EAB	-0.4297	1.4879	-2.4045	1.5971	-0.6258	0.9536	0.2606	0.3471	1.1466
SSUSI F17			2.0334	1.4879	-2.4045	1.5971	-0.6258	0.9536	0.2606	0.3471	1.1466
SSUSI F18			0.0999	1.4879	-2.4045	1.5971	-0.6258	0.9536	0.2606	0.3471	1.1466
SSUSI F19			-0.4215	1.4879	-2.4045	1.5971	-0.6258	0.9536	0.2606	0.3471	1.1466
SSUSI F16		OCB	0.6026	-0.1638	1.0985	1.1386	-1.7874	0.3829	0.8246	0.2788	0.3755
SSUSI F17			0.9150	-0.1638	1.0985	1.1386	-1.7874	0.3829	0.8246	0.2788	0.3755
SSUSI F18			0.4633	-0.1638	1.0985	1.1386	-1.7874	0.3829	0.8246	0.2788	0.3755
SSUSI F19			0.5523	-0.1638	1.0985	1.1386	-1.7874	0.3829	0.8246	0.2788	0.3755
SSUSI F16	LBHL	EAB	0.8471	-1.1343	0.9011	1.1750	-0.5542	0.1354	0.3850	-0.4534	-0.5136
SSUSI F17			-0.5002	-1.1343	0.9011	1.1750	-0.5542	0.1354	0.3850	-0.4534	-0.5136
SSUSI F18			0.8319	-1.1343	0.9011	1.1750	-0.5542	0.1354	0.3850	-0.4534	-0.5136
SSUSI F19			-0.6564	-1.1343	0.9011	1.1750	-0.5542	0.1354	0.3850	-0.4534	-0.5136
SSUSI F16		OCB	0.1762	0.4296	2.5027	0.4913	-1.7602	0.0846	0.3539	-0.0834	-0.3163
SSUSI F17			0.7200	0.4296	2.5027	0.4913	-1.7602	0.0846	0.3539	-0.0834	-0.3163
SSUSI F18			-0.2955	0.4296	2.5027	0.4913	-1.7602	0.0846	0.3539	-0.0834	-0.3163
SSUSI F19			-0.2739	0.4296	2.5027	0.4913	-1.7602	0.0846	0.3539	-0.0834	-0.3163

4 Validation

The corrected GUVI and SSUSI OCB estimations were validated against the DMSP CRB measurements described in Section 2.2.3. As there are 5 years of GUVI data and 10 years of SSUSI data paired with DMSP CRBs, there are significant differences in the number of pairs available for validation. The estimated OCB locations were paired to CRB locations that occurred within 10 min UT and 15 min MLT. Both hemispheres and all DMSP spacecraft have been combined, to ensure that there are enough pairs for meaningful statistics. Figures 8 and 9 show the validation results for the two different LBH channels. These validation results provide confidence in both the ALB detection process and the functional descriptions of the offsets between the ALB and the DMSP particle precipitation boundaries.

The GUVI validation results for both wavelengths are similar, with biases of approximately 1° in the median and mean difference. These biases are larger than those previously found for IMAGE and AMPERE, which are on the order of 0.1° (Burrell et al., 2020; Chisham et al., 2022). However, the standard deviation is similar (for LBHS) or lower (for LBHL).

https://doi.org/10.5194/egusphere-2026-5594
Preprint. Discussion started: 6 November 2026
© Author(s) 2026. CC BY 4.0 License.

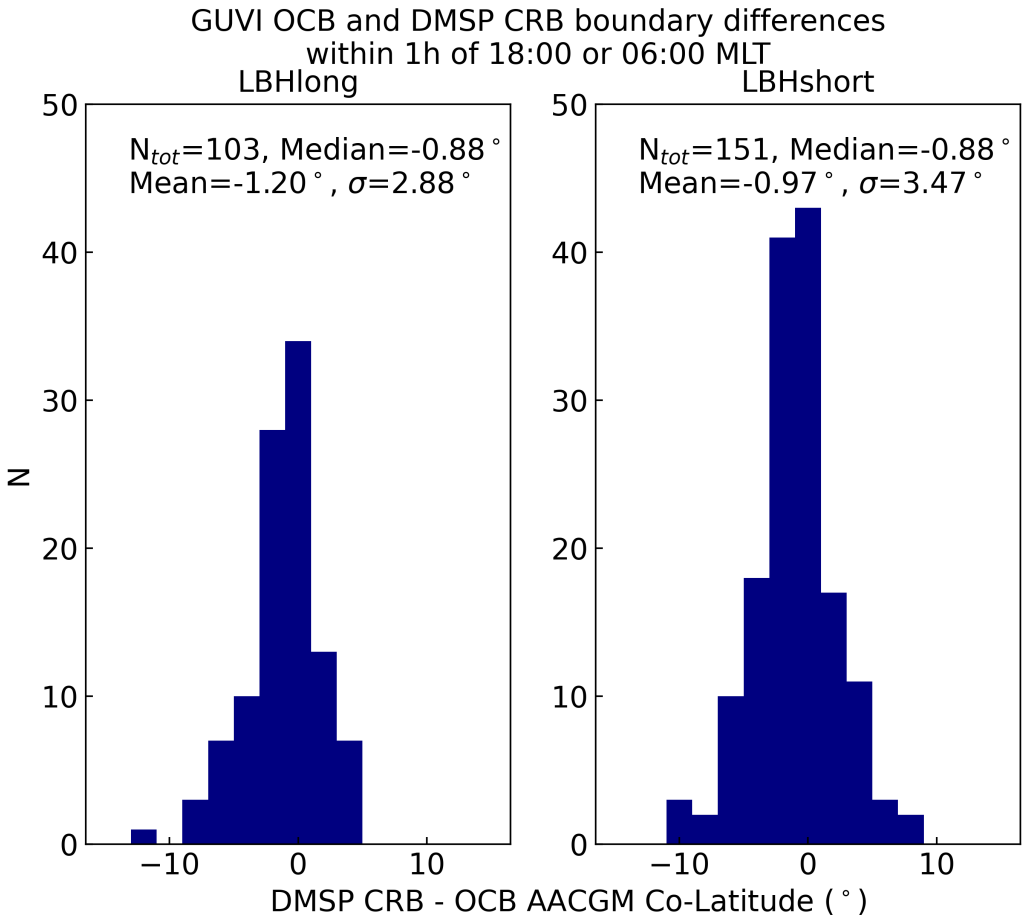


Figure 8. Histograms of differences between the DMSP CRB locations from DMSP F13, F15, F16, and F17 and the GUVI OCB for times within 05:00-07:00 MLT and 17:00-19:00 MLT. The left column shows the results for the LBHL channel and the right column shows the LBHS channel combining data from the northern and southern hemisphere.

https://doi.org/10.5194/egusphere-2026-5594
Preprint. Discussion started: 6 November 2026
© Author(s) 2026. CC BY 4.0 License.

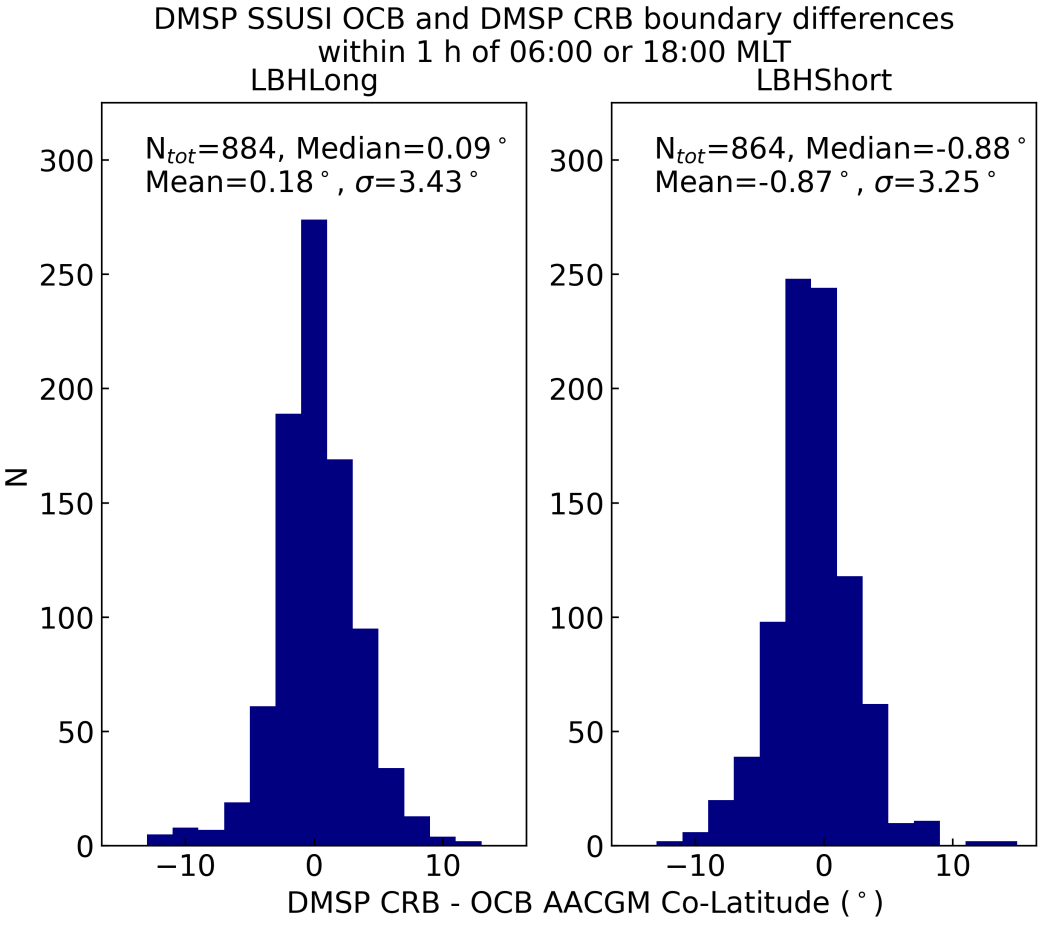


Figure 9. Histograms of differences between the DMSP CRB locations from DMSP F13, F15, F16, F17, and F18 and the DMSP SSUSI OCB from F16, F17, F18, and F19 for times within 05:00-07:00 MLT and 17:00-19:00 MLT. The left column shows the results for the LBHL channel and the right column shows the LBHS channel combining data from the northern and southern hemisphere.

https://doi.org/10.5194/egusphere-2026-5594
Preprint. Discussion started: 6 November 2026
© Author(s) 2026. CC BY 4.0 License.

The SSUSI validation results are significantly better for LBHL than for LBHS. The SSUSI LBHL median and standard deviation are the same order of magnitude as those for IMAGE and AMPERE, though the mean is slightly larger. The SSUSI LBHS results are similar to the GUVI LBHS results.

5 Conclusions

This study presents poleward and equatorward auroral luminosity boundary estimates from the TIMED GUVI and DMSP SSUSI FUV instruments at two wavelength bands: Lyman-Birge-Hopfield Short and Long. A functional relationship between the poleward ALB and the OCB is established, as well as between the equatorward ALB and the EAB. While the TIMED GUVI field-of-view was large enough to establish these relationships independently, the DMSP SSUSI observations were combined for the four different satellites to provide the greatest possible MLT coverage. Individual offsets between the SSUSI ALBs and the OCB/EAB were then calculated for each satellite, which showed differences of about half a degree.

The performance of the OCB estimation was validated against an independent proxy, the convection reversal boundary. The validation shows that both the GUVI and SSUSI fits perform better in the LBHL wavelength channel than in the LBHS channel. However, the difference is small enough that both are suitable for research.

Modelling and statistical studies of the atmosphere-ionosphere-magnetosphere system at high latitudes should avoid mixing data from inside the polar cap, the auroral oval, and the sub-auroral region. Each of these areas are characterised by distinct coupling processes and mixing data from the different regions will contaminate scientific studies that look into long-term behaviour or examine connections between the different spheres within the geospace system (Chisham, 2017; Chisham et al., 2025). While the MLT coverage of the GUVI and SSUSI data sets are not large enough on their own to provide a full set of hemispheric boundaries, they may be used to aid more focused studies. They could also be used to adjust assimilative models of the OCB or EAB.

Code and data availability. For this study, the high-resolution imaging data files from TIMED GUVI and DMSP SSUSI were obtained from NASA SPDF (https://spdf.gsfc.nasa.gov/pub/data/). Poleward and equatorward ALBs were obtained for this time period from the LBHS and LBHL spectral bands using pyIntensityFeatures (Burrell et al., 2026b). These ALBs may be accessed online from Zenodo (Burrell and Zawdie, 2026; Burrell et al., 2026a).

Author contributions. AB conceptualized this study, curated and analysed data (taking the lead on the SSUSI boundary functions and the validation for both GUVI and SSUSI), designed the methodology, created and published the software, contributed to the visualization, and wrote the original draft of the manuscript. GC contributed to the conceptualization, curated and analysed data (taking the lead on the GUVI boundary functions), designed the methodology, and contributed to the visualization of this study as well as the editing of the manuscript. Y-JC performed data analysis (provided the DMSP CRBs and insight into their appropriate use) and contributed to the editing of this manuscript.

https://doi.org/10.5194/egusphere-2026-5594
Preprint. Discussion started: 6 November 2026
© Author(s) 2026. CC BY 4.0 License.

BF contributed to the analysis of the SSUSI ALBs and the editing of this manuscript. KZ acquired funding to support this publication and contributed to the editing of this manuscript.

Competing interests. The authors have no competing interests.

Acknowledgements. The GUVI data used here are provided through support from the NASA MO&DA program. The GUVI instrument was designed and built by The Aerospace Corporation and The Johns Hopkins University. The Principal Investigator is Dr. Larry J. Paxton.

This Defense Meteorological Satellite Program (DMSP) satellite data is provided through CDAWeb.

AB, BF, and KZ are supported by the Office of Naval Research.

GC was supported by the UK Natural Environment Research Council (NERC) highlight topic grant NE/W003066/1 (FINESSE). He was also funded as part of the British Antarctic Survey (BAS) Polar Science for a Sustainable Planet Programme, funded by NERC.

Y-JC was partially supported by NASA Living with a Star Grant 80NSSC20K1775.

https://doi.org/10.5194/egusphere-2026-5594
Preprint. Discussion started: 6 November 2026
© Author(s) 2026. CC BY 4.0 License.

References

Akasofu, S.-I.: The Auroral Oval, The Auroral Substorm, and their Relations witht he Internal Structure of the Magnetosphere, Planet. Space Sci., 14, 587–595, 1966.

Boakes, P. D., Milan, S. E., Abel, G. A., and Freeman, M. P.: On the use of IMAGE FUV for estimating the latitude of the open/closed magnetic field line boundary in the ionosphere, Annales Geophysicae, 26, 2759–2769, https://doi.org/10.5194/angeo-26-2759-2008, 2008.

Borovsky, J. E. and Valdivia, J. A.: The Earth's Magnetosphere: A Systems Science Overview and Assessment, 39, 817–859, https://doi.org/10.1007/s10712-018-9487-x, 2018.

Burrell, A. and Zawdie, K.: GUVI Auroral Luminosity Boundary Files, https://doi.org/10.5281/zenodo.22238096, 2026.

Burrell, A., Fritz, B., and Zawdie, K.: SSUSI Auroral Luminosity Boundary Files, https://doi.org/10.5281/zenodo.22258434, 2026a.

Burrell, A. G., van der Meeren, C., and Laundal, K. M.: aacgmv2: v2.4.1, https://doi.org/10.5281/zenodo.1212695, 2018.

Burrell, A. G., Chisham, G., Milan, S. E., Kilcommons, L., Chen, Y.-J., Thomas, E. G., and Anderson, B.: AMPERE polar cap boundaries, Annales Geophysicae, 38, 481–490, https://doi.org/10.5194/angeo-38-481-2020, 2020.

Burrell, A. G., Chisham, G., Longden, N., Fritz, B., and Zawdie, K. A.: Automated Identification of Auroral Luminosity Boundaries Using pyIntensityFeatures, Journal of Geophysical Research: Space Physics, 130, https://doi.org/10.1029/2025ja034230, 2025.

Burrell, A. G., Longden, N. S., and Chisham, G.: aburrell/pyIntensityFeatures: Version 0.2.0, https://doi.org/10.5281/zenodo.19135203, 2026b.

Carbary, J. F., Sotirelis, T., Newell, P. T., and Meng, C.-I.: Auroral boundary correlations between UVI and DMSP, Journal of Geophysical Research, 108, 1018, https://doi.org/10.1029/2002JA009378, 2003.

Chen, Y.-J. and Heelis, R. A.: Motions of the Convection Reversal Boundary and Local Plasma in the High-Latitude Ionosphere, Journal of Geophysical Research: Space Physics, 123, 2953–2963, https://doi.org/10.1002/2017ja024934, 2018.

Chen, Y.-J., Heelis, R. A., and Cumnock, J. A.: Response of the ionospheric convection reversal boundary at high latitudes to changes in the interplanetary magnetic field, Journal of Geophysical Research: Space Physics, 120, 5022–5034, https://doi.org/10.1002/2015ja021024, 2015.

Chisham, G.: A new methodology for the development of high-latitude ionospheric climatologies and empirical models, Journal of Geophysical Research: Space Physics, 122, 932–947, https://doi.org/10.1002/2016JA023235, 2017.

Chisham, G., Burrell, A. G., Thomas, E. G., and Chen, Y.-J.: Ionospheric Boundaries Derived From Auroral Images, Journal of Geophysical Research: Space Physics, 127, e2022JA030 622, https://doi.org/10.1029/2022ja030622, 2022.

Chisham, G., Burrell, A. G., and Zawdie, K. A.: The Impact of Adaptive High-Latitude Coordinates, Geophysical Research Letters, 52, https://doi.org/10.1029/2025gl115265, 2025.

Cowley, S. W. H. and Lockwood, M.: Excitation and decay of solar-wind driven flows in the magnetosphere-ionosphere system, Annales Geophysicae, 10, 103–115, 1992.

Decotte, M., Laundal, K. M., Hatch, S. M., and Reistad, J. P.: Auroral Oval Morphology: Dawn-Dusk Asymmetry Partially Induced by Earth's Rotation, Journal of Geophysical Research: Space Physics, 128, e2023JA031 345, https://doi.org/10.1029/2023ja031345, 2023.

Dungey, J. W.: Interplanetary Magnetic Field and the Auroral Zones, Physical Review Letters, 6, 47–48, 1961.

Hall, R. C.: A History of the Military Polar Orbiting Meteorological Satellite Program, Tech. rep., Office of the Historian, National Reconnaissance Office, 2001.

https://doi.org/10.5194/egusphere-2026-5594
Preprint. Discussion started: 6 November 2026
© Author(s) 2026. CC BY 4.0 License.

Kilcommons, L., Redmon, R., and Knipp, D.: Defense Meteorology Satellite Program (DMSP) Electron Precipitation (SSJ) Auroral Boundaries, 2010-2014, https://doi.org/10.5281/zenodo.3373812, 2019.

Kilcommons, L. M., Redmon, R. J., and Knipp, D. J.: A new DMSP magnetometer and auroral boundary data set and estimates of field-aligned currents in dynamic auroral boundary coordinates, Journal of Geophysical Research: Space Physics, 122, 9068–9079, https://doi.org/10.1002/2016ja023342, 2017.

Klenzing, J., Burrell, A. G., Stoneback, R., Smith, J., Navarro, L., Esman, T., Govada, A., Pembroke, A., and Spence, C.: pysat/pysatNASA: v0.0.6, https://doi.org/10.5281/zenodo.13888100, 2024.

Longden, N., Chisham, G., Freeman, M. P., Abel, G. A., and Sotirelis, T.: Estimating the location of the open-closed magnetic field line boundary from auroral images, Annales Geophysicae, 28, 1659–1678, https://doi.org/10.5194/angeo-28-1659-2010, 2010.

Mukhopadhyay, A., Panovska, S., Garvey, R., Liemohn, M. W., Ganjushkina, N., Brenner, A., Usoskin, I., Balikhin, M., and Welling, D. T.: Wandering of the auroral oval 41,000 years ago, Science Advances, 11, https://doi.org/10.1126/sciadv.adq7275, 2025.

Newell, P. T., Burke, W. J., Sanchez, E. R., Meng, C.-I., Greenspan, M. E., and Clauer, C. R.: The low-latitude boundary layer and the boundary plasma sheet at low altitude: Prenoon precipitation regions and convection reversal boundaries, J. Geophys. Res., 96, 21 013–21 023, 1991.

Newell, P. T., Feldstein, Y. I., Galperin, Y. I., and Meng, C.-I.: Morphology of nightside precipitation, J. Geophys. Res., 101, 10 737–10 748, 1996.

Newell, P. T., Ruohoniemi, J. M., and Meng, C.-I.: Maps of precipitation by source region, binned by IMF, with inertial convection streamlines, Journal of Geophysical Research, 109, A10 206, https://doi.org/10.1029/2004JA010499, 2004.

Paxton, L. J., Morrison, D., Zhang, Y., Kil, H., Wolven, B., Ogorzalek, B. S., Humm, D., and Meng, C.-I.: Validation of Remote Sensing Products Produced by the Special Sensor Ultraviolet Scanning Imager (SSUSI)- a Far-UV Imaging Spectrograph on DMSP F16, in: Optical Spectroscopic Techniques, Remote Sensing, and Instrumentation for Atmospheric and Space Research IV, edited by Larar, A. M. and Mlynczak, M. G., vol. 4485, 2002.

Paxton, L. J., Christensen, A. B., Morrison, D., Wolven, B., Kil, H., Zhang, Y., Ogorzalek, B. S., Humm, D. C., Goldsten, J., DeMajistre, R., and Ming, C.-I.: GUVI: A Hyperspectral Imager for Geospace, in: Instruments, Science and Methods for Geospace and Planetary Remote Sensing, edited by Nardell, C. A., Lucey, P. G., Yee, J.-H., and Garvin, J. B., vol. 5660, pp. 228–240, https://doi.org/10.1117/12.579171, 2004.

Shepherd, S. G.: Altitude-adjusted corrected geomagnetic coordinates: Definition and functional approximations, Journal of Geophysical Research: Space Physics, 119, 7501–7521, https://doi.org/10.1002/2014JA020264, 2014.

Troyer, R. N., Landry, R., David, M., Eccles, J. V., and Acosta, A. E.: A Probabilistic *Kp* and *Hp* Driven Auroral Boundary Model Using 28 Years of DMSP Data, Journal of Geophysical Research: Space Physics, 130, https://doi.org/10.1029/2024ja033497, 2025.

Yee, J.-H., Cameron, G. E., and Kusnierkiewicz, D. Y.: An Overview of TIMED, in: SPIE Conference on Optical Spectroscopic Techniques and Instrumentation for Atmospheric and Space Research III, vol. 3756, pp. 244–254, https://doi.org/10.1117/12.366378, 1999.